Computers and Electronics in Agriculture 136 (2017) 166–175

Contents lists available at ScienceDirect

Computers and Electronics in Agriculture

journal homepage: www.elsevier.com/locate/compag

Original papers

Total station data assessment using an industrial robotic arm for dynamic 3D in-field positioning with sub-centimetre accuracy

Dimitris S. Paraforos [a,*], Marcus Reutemann [b], Galibjon Sharipov [a], Roland Werner [b], Hans W. Griepentrog [a]

[a] University of Hohenheim, Institute of Agricultural Engineering 440d, Garbenstr. 9, D-70599 Stuttgart, Germany
[b] John Deere GmbH & Co. KG, Intelligent Solutions Group, Advanced Engineering, Straβburger Allee 3, D-67657 Kaiserslautern, Germany

ARTICLE INFO

Article history:
Received 1 October 2016
Received in revised form 10 March 2017
Accepted 12 March 2017
Available online 22 March 2017

Keywords:
Total station
Robotic arm
3D positioning
Cross-track error
In-field accuracy

ABSTRACT

For agricultural tasks related to precision farming, accurate in-field positioning is a necessity. The accuracy of some centimetres that the real time kinematic-global navigation satellite system (RTK-GNSS) can provide is adequate for many applications, such as auto-steering navigation and section control for spraying or fertiliser applications. Nevertheless, the demand for higher in-field accuracy at a mm level is increasing. A device that is gaining a lot of attention in the agricultural sector for its increased accuracy is a robotic total station (TS) that can track a prism mounted on a vehicle. With the aim to be able to use this device under realistic conditions for dynamic 3D in-field positioning at a sub-centimetre level, the accuracy of the TS was assessed utilising an industrial robotic arm. The robotic arm had a repeatability factor of ±0.1 mm and was placed outdoors under normal environmental conditions for agriculture practice. Straight AB lines but also U-turn and Pattern-8 experiments were performed. The absolute error of the robotic arm had a maximum mean value of 0.33 mm for the Pattern-8 experiment, while the highest error, equal to 1.30 mm, was detected in the 95th percentile of the same experiment. The horizontal and vertical relative cross-track error (XTE) between the TS and the robotic arm data was calculated for various speeds and for two different positions of the TS. From the results, it was evident that as the speed increased so did the horizontal relative XTE. Furthermore, changing the position of the TS from in line to perpendicular, in respect to the direction of motion, proved to result in a higher accuracy. The maximum mean horizontal relative XTE value of all experiments was 4.01 mm for Pattern-8, which also had the maximum value for the 95th percentile, i.e. 12.86 mm. The vertical relative XTE for all experiments did not exceed 10 mm including the outliers.

1. Introduction

Accurate in-field positioning of agricultural vehicles is a prerequisite in order to perform applications related to precision farming. Over the last decades, the use of real time kinematic-global navigation satellite system (RTK-GNSS), which offers position accuracy at the cm level, has widely expanded introducing new possibilities to agricultural applications. One of the most important was the development and later the widespread use of the auto-steering systems, which have thoroughly been assessed for their accuracy (Easterly et al., 2010; ISO, 2012). Using this satellite-based method, agricultural-related spatial data were possible to be acquired and analysed producing valuable information for real-time applications such as section control and variable dose rate of fertiliser and pesticide applications, and yield mapping.

Nevertheless, there has been always a demand for even more accurate in-field positioning at the mm level. The RTK-GNSS is not accurate enough, especially in the vertical direction. This level of accuracy is necessary when aiming to increase the level of automation in agricultural tasks. An example is the area of plant phenotyping using autonomous vehicles (Ruckelshausen et al., 2009), where data fusion from various sensors are used to create a three-dimensional (3D) reconstruction of crop plants. Although vision systems have been developed aiming to provide such a high accuracy by fusing information from different images, usually a positioning system is utilised to georeference each acquired image (Rose et al., 2016). Consequently, a more accurate positioning system would result in a more realistic final 3D plant reconstruction. Another important agricultural-related area with a demand on high accuracy at that level is the development of methodologies for crop protection, such as seed and plant mapping (Griepentrog et al., 2005) or mechanical weeding (Nørremark et al., 2008).

* Corresponding author.
E-mail address: d.paraforos@uni-hohenheim.de (D.S. Paraforos).

http://dx.doi.org/10.1016/j.compag.2017.03.009
0168-1699/

A device with a higher accuracy than an RTK-GNSS is a total station (TS), which could be utilised to provide position data when this level of accuracy is demanded. Commonly, this device is used in the domain of civil engineering and provides a higher accuracy compared to satellite-based positioning systems. A TS is an optical instrument, measuring horizontal and vertical angles, as well as slope distances, from the TS to target points of interest (POIs) in a 3D polar coordinate system. During measurement, the POIs are generally marked with prisms, which serve as reflecting targets for angular and electronic distance measurements. By setting up the TS and measuring a number of known ground control points, the prism location information can be transformed to absolute coordinates in a predefined geodetic coordinate reference system. New robotic TSs offer the possibility to track dynamically a prism mounted on an agricultural vehicle. The data output rate can reach up to 20 Hz, similar to one of most commercial RTK-GNSS receivers. The only restriction is that there should always be a line of sight between the TS and the prism.

The use of a TS for accurate 3D positioning related to agricultural applications is increasing the last years. This can be seen from the research papers that are being published and utilise TSs for ground-truth. Liu and Noguchi (2016) used it for assessing the positioning of an unmanned surface vehicle (USV) for autonomous navigation in a paddy field. The dynamic position of a robot in a poultry house was quantitatively evaluated by Vroegindeweij et al. (2016) using the information from a TS as the ground-truth. In a study by Vougioukas et al. (2016), the TS was used for assessing an ultra-wideband radio-based system for worker localisation in orchards.

The TS has been also used in plant phenotyping applications as Garrido et al. (2015) mounted three LiDARs (light detection and ranging), with a different viewing angle, on a small autonomous robot for 3D maize plant reconstruction. There, the TS was providing the geo-reference for overlapping the LiDAR point clouds. Forest area management and tree height measurements have been widely performed utilising a TS. The tree height and the height of the crown base were measured using a TS by Xu et al. (2013) while Yan et al. (2012) utilised a no prism TS to measure 3D coordinates, diameter of the trunk, tree height and crown width of *Pinus tabuliformis* trees.

A number of studies were conducted trying to assess the accuracy of GNSS-based solutions using a TS as a benchmark. In a research by Parent et al. (2008), one of the objectives was to evaluate a GNSS-embedded method for field digital elevation models compared to measurements from a TS. The TS has been also used to assess the accuracy of auto-steering systems (Gavric et al., 2011; Groth et al., 2013). An important issue regarding data synchronisation when assessing the GNSS with a TS was discussed by Sama et al. (2013) and a hardware method for time-stamping these asynchronous data was introduced. The question that arises is if the TS can replace the GNSS for accurate in-field 3D dynamic positioning. In a recent research by Paraforos et al. (2015) the TS was utilised to assess in-field positioning provided by RTK-GNSS and inertial measurement unit (IMU) fused data. It was concluded that the TS could also be used for carrying out precision agriculture-related applications that require high accuracy. Nevertheless, this high accuracy of the TS needs to be determined and quantified under realistic conditions.

The aim of the paper is to assess the 3D accuracy of a TS from an agricultural-related perspective, in order to be used for dynamic in-field positioning when sub-centimetre accuracy is required, but also when a satellite-based solution is not available due to reflection or shading errors caused by high trees or buildings. The novelty of the presented methodology lies in the fact that it examines the accuracy of the TS measurements under dynamic and realistic outdoor conditions, compared to indoor laboratory environment like previous studies (Kirschner and Stempfhuber, 2008). Furthermore, except straight AB lines, other patterns are examined, i.e. U-turn and Pattern-8, which are usually followed when performing in-field agricultural-related tasks. The first is widely used under field working conditions for headland turning, while in some cases the tractor operators perform the latter for obstacle avoidance, e.g. while swathing grass (Paraforos et al., 2014).

2. Materials and methods

2.1. Instrumentation

To develop a methodology for assessing the TS dynamic 3D position accuracy under outdoor conditions, a TX200L robotic arm (Stäubli International AG, Pfäffikon, Switzerland) was utilised. The specific robotic arm is placed on the rooftop of the John Deere European Technology Innovation Centre (Kaiserslautern, Germany). The robotic arm has six degrees of freedom and a repeatability factor of a selected path, according to ISO 9283 (ISO, 1998), of ±0.1 mm. A Trimble SPS930 (Trimble, Sunnyvale, USA) universal TS was placed outside the robotic arm platform to track a Trimble MT900 prism mounted on the end effector of the robotic arm (Fig. 1). The main technical characteristics of the SPS930 TS are summarised in Table 1. The assessing device should have at least 4 times higher accuracy (4:1 test accuracy ratio (TAR)) for the results to be reliable (ANSI/NCSL, 2006), while usually a TAR of 10:1 is preferable. The utilised robotic arm, which is widely used in industrial applications, could provide this level of TAR.

2.2. Experimental design

The experimental design is presented in Fig. 2. Initially, an AB line was performed with three different speeds, i.e. 50 mm s^{-1}, 200 mm s^{-1}, and 500 mm s^{-1}. For these measurements, the TS was placed in the same line as the AB line (Fig. 2a). The AB line with a speed of 500 mm s^{-1} was repeated but this time the TS was placed perpendicular to the AB line (Fig. 2b). Without moving the TS, the speed of the robotic arm was increased to 1000 mm s^{-1} and, both a U-turn and a Pattern-8 experiment were performed as can be seen in Fig. 2c and d, respectively. The green arrows in Fig. 2 indicate the starting point and direction of each experiment. The physical limitations of the robotic arm links did not allow long lengths to be examined. In the performed experiments it was 3.600 m, 8.540 m, and 12.077 m, for the AB line, U-turn, and Pattern-8 experiment, respectively.

The coordinate frame of the robotic arm $O(x, y, z)$, which is illustrated in Fig. 2a, is indicating the origin and the direction of the positive values of the three axes (the z axis was pointing upwards), and was the same for all performed experiments. The data acquisition software of the robotic arm was configured to provide the position data of the same point where the prism was attached on. A built-in option of the robotic arm allowed to specify a tool offset that was automatically applied to the end effector position. Consequently, the offset in all three dimensions x, y, and z, between the centre of the prism and the end effector of the robotic arm, was measured and imported in the software.

The Trimble SCS900 Site Controller software, running on a Trimble Yuma 2 tablet computer, was used to acquire and store data from the TS. In order to have all measurements of the TS in the same coordinate frame (robotic arm frame), independently of its position, the TS was stationed using the known coordinates of the points A and B. By placing the prism at these points and by inserting the corresponding x, y, and z values of the robotic arm to the SCS900 software of the TS, a rigid transformation was per-

Fig. 1. Utilised instrumentation (photo: John Deere GmbH & Co. KG, Intelligent Solutions Group, Advanced Engineering, modified).

Table 1
SPS 930 TS technical data.

Parameter	Value
Distance measurement accuracy	±(4 mm + 2 ppm)
Angle measurement horizontal and vertical accuracy	0.3 mgon
Measurement range	2500 m
Data output rate	20 Hz
Maximum radial speed of target	114° s^{-1}
Maximum axial speed of target	6 m s^{-1}
Synchronized measurement data	<1 ms

formed that transformed all subsequent measured points by the TS, to the *O* frame. This procedure was also followed for the performed experiments of Fig. 2c and d, where the TS was initially stationed with the coordinates of points A and B and then the prism was moved to the starting point U and S, respectively. The 3D position data were transmitted from the TS as long as the current measurement varied at least by 1 mm from the previous one but with a maximum frequency of 20 Hz.

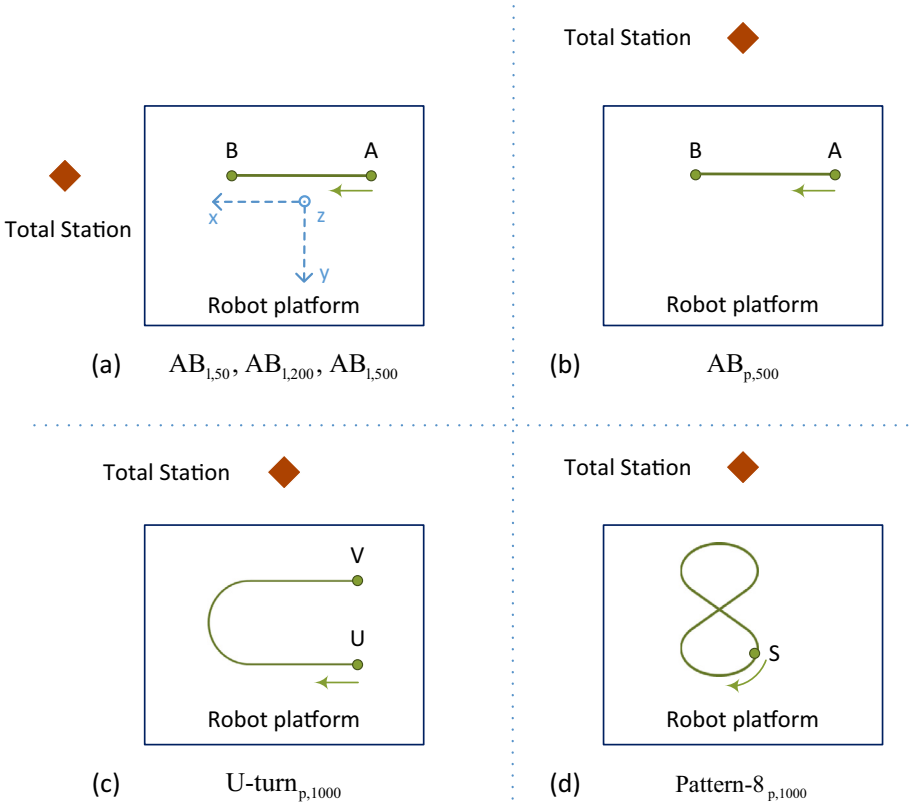

Fig. 2. Performed experiments: (a) AB line with 50 mm s^{-1}, 200 mm s^{-1}, and 500 mm s^{-1} and the TS placed in the same line, (b) AB line with 500 mm s^{-1} and the TS placed perpendicular to the AB line, (c) U-turn with 1000 mm s^{-1}, and (d) Pattern-8 with 1000 mm s^{-1}. The green arrows indicate the starting point and direction of each experiment. (For interpretation of the references to colour in this figure legend, the reader is referred to the web version of this article.)

Table 2
Summary of all performed experiments.

Acronym	Type of experiment	TS position	Speed (mm s^{-1})	Repetitions
$AB_{l,50}$	AB line	In line with AB	50	6 (3 from A to B and 3 from B to A)
$AB_{l,200}$	AB line	In line with AB	200	20 (10 from A to B and 10 from B to A)
$AB_{l,500}$	AB line	In line with AB	500	20 (10 from A to B and 10 from B to A)
$AB_{p,500}$	AB line	Perpendicular to AB	500	20 (10 from A to B and 10 from B to A)
U-$turn_{p,1000}$	U-turn	Perpendicular to AB	1000	20 (10 from U to V and 10 from V to U)
Pattern-$8_{p,1000}$	Pattern-8	Perpendicular to AB	1000	10 (Starting and finishing at S)

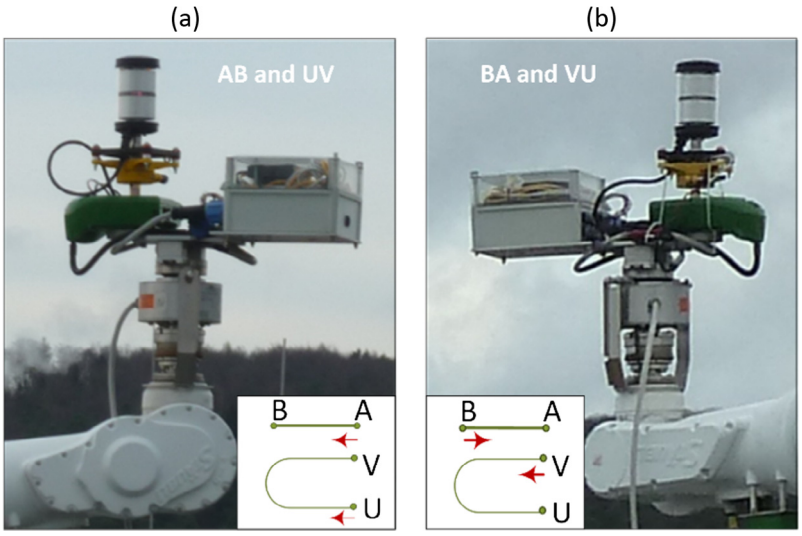

Fig. 3. Rotation by 180 degrees around the vertical axis for performing the (a) AB and UV, and (b) BA and VU. (photos: John Deere GmbH & Co. KG, Intelligent Solutions Group, Advanced Engineering, modified).

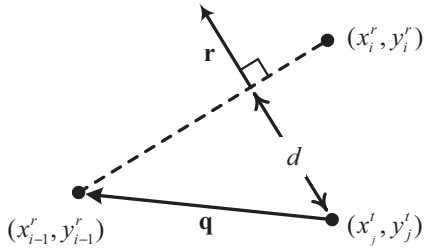

Fig. 4. Geometrical representation for calculating the 2D distance of the measured by the TS prism positions $p_j^t = (x_j^t, y_j^t)$ from a line connecting the two reference points $p_{i-1}^r = (x_{i-1}^r, y_{i-1}^r)$ and $p_i^r = (x_i^r, y_i^r)$ as they were provided by the robotic arm.

For all experiments, the robotic arm was programmed to have a constant value on the *z*-axis. This value was determined according to the specific robotic arm dimensions and was set to 1579.45 mm for all AB lines and the U-turn measurements, and to 1379.45 mm for the Pattern-8 experiment. This change of 200 mm was necessary in order to have the entire Pattern-8 path inside robot's working area. A summary of all performed tests and the number of the repetitions of each experiment can be seen in Table 2.

An important aspect of the robotic arm was that the end effector (position of the prism) was rotating by 180 degrees around its vertical axis when it was necessary to change the direction of travel at the end point of the paths. This was taking place at points B and V for all AB lines and U-turn, respectively. Fig. 3a is presenting the configuration of the end effector of the robotic arm for AB and UV, while in Fig. 3b the end effector of the robotic arm is rotated by

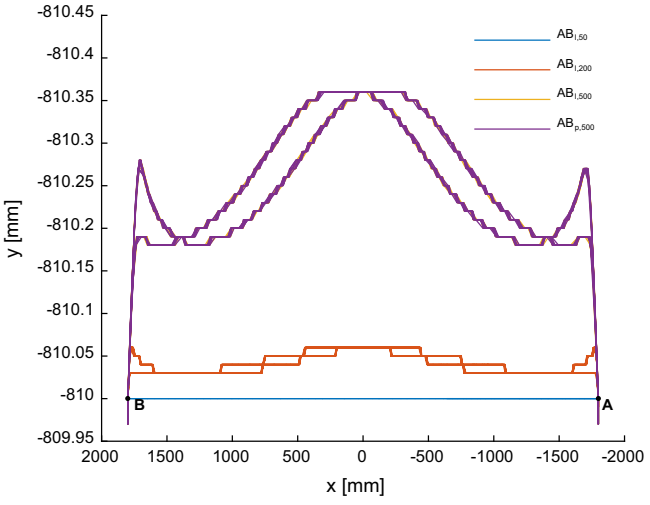

Fig. 5. Position of the robotic arm end effector in the *xy*-plane for all AB line measurements. Points A and B are also indicated (·).

Table 3
Absolute error of the robotic arm end effector in the *xy*-plane for the AB lines.

Experiment	Mean (mm)	Standard deviation (mm)	95th percentile (mm)
$AB_{l,50}$	0.00	0.00	0.00
$AB_{l,200}$	0.01	0.02	0.06
$AB_{l,500}$	0.06	0.11	0.32
$AB_{p,500}$	0.06	0.11	0.32

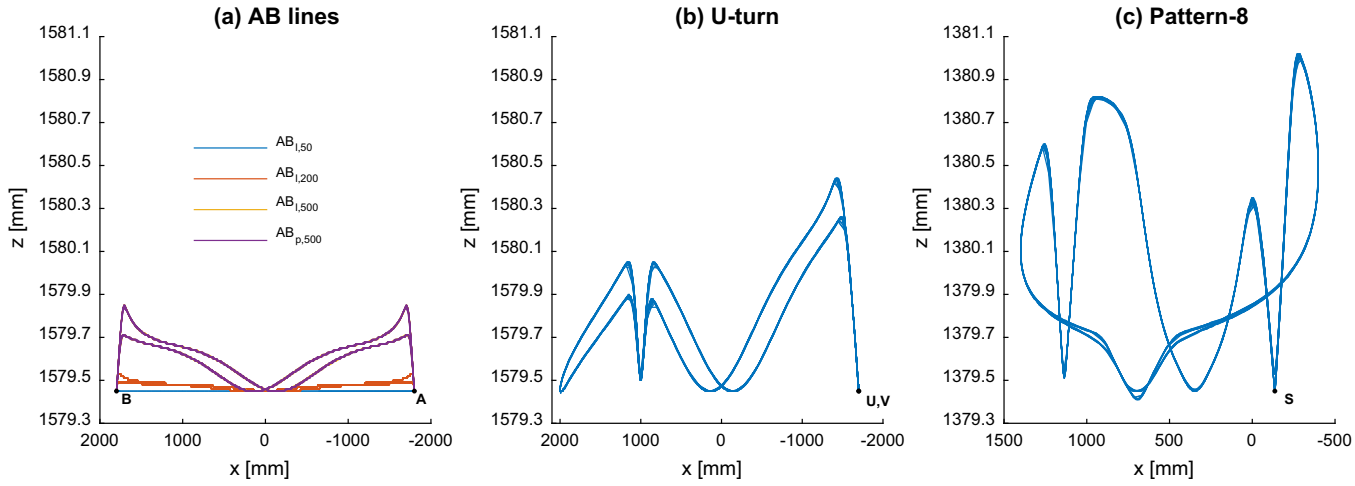

Fig. 6. Position of the robotic arm end effector in the *xz*-plane for (a) AB lines, (b) U-turn, and (c) Pattern-8 measurements. Points A, B, U, V, and S are also indicated (·).

Table 4
Absolute error of the robotic arm end effector in the *xz*-plane for all experiments.

Experiment	Mean (mm)	Standard deviation (mm)	95th percentile (mm)
$AB_{l,50}$	0.00	0.00	0.00
$AB_{l,200}$	0.01	0.02	0.04
$AB_{l,500}$	0.03	0.08	0.22
$AB_{p,500}$	0.03	0.08	0.22
$U\text{-turn}_{p,1000}$	0.14	0.23	0.65
$Pattern\text{-}8_{p,1000}$	0.33	0.43	1.30

180 degrees for performing BA and VU. The direction of travel was not necessary to change for the Pattern-8 experiment as point S was both the starting and ending point.

2.3. Noise removal in TS position data

A Butterworth low-pass filter with a cut-off frequency of 4 Hz was applied to remove noise in the TS position data. For the AB line experiments, a first order filter was implemented in all three directions (x, y, z), while for the U-turn and Pattern-8 experiments a first order filter was utilised only on the z-axis position data. On the x and y-axes position data of these two experiments a second order filter was used as the paths on the xy-plane had turning sections, which required this order increase of the filter.

2.4. Robotic arm performance

The capability of the robotic arm to follow the desired paths of Fig. 2 was examined independently from the TS measurements, by analysing the obtained data from the data acquisition software of the robotic arm. The aim was to assess the performance of the control algorithm of the robotic arm as the speed and the direction was varying. A direct comparison of the position data of the end effector of the robotic arm in the xy-plane was possible only for the AB lines as for these experiments the value on the y-axis was constant. In the case of the xz-plane, since the value of the z-axis was configured to be constant for all experiments, a comparison between all experiments of the position deviation from the desired value was possible.

2.5. Accuracy assessment

There are several methods to assess dynamic position data accuracy. One method is to calculate the shortest distance between a recorded position and a fitted line of the data from the assessing device. In this paper, the relative cross-track error (XTE) was chosen as an accuracy assessment criterion for the TS data, as it is a common method for assessing positioning systems (Han et al.,

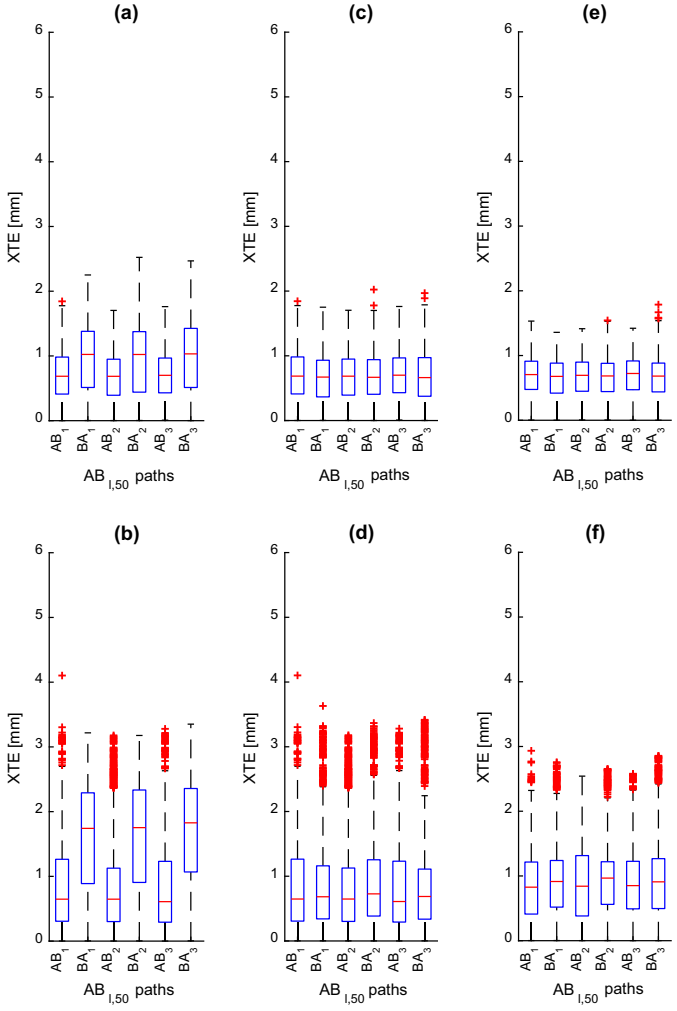

Fig. 7. $AB_{l,50}$ boxplots for (a) horizontal and (b) vertical relative XTE. The same information after the systematic error removal ((c) and (d)), and after the implementation of the Butterworth low-pass filter ((e) and (f)).

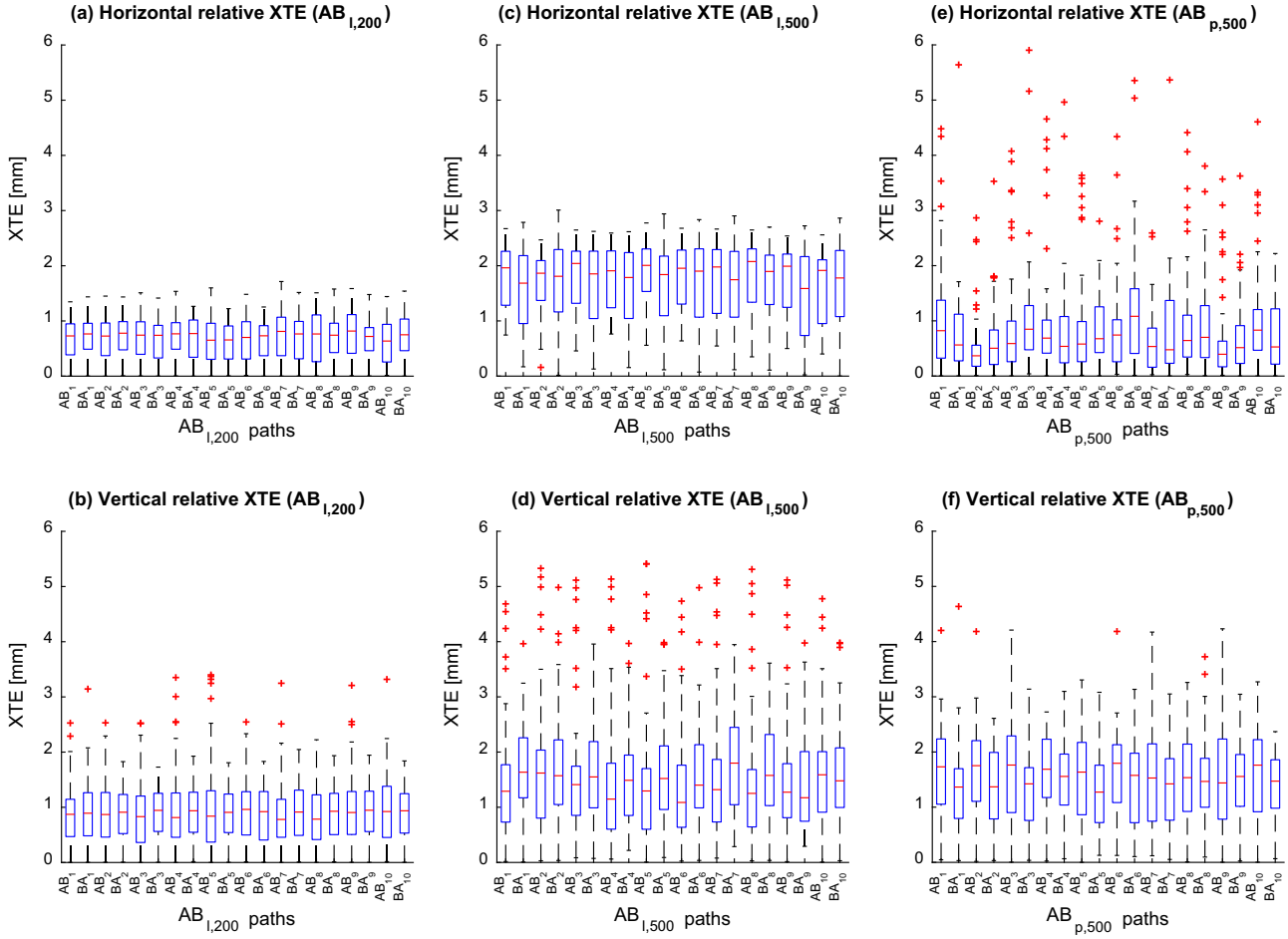

Fig. 8. Boxplots for horizontal and vertical relative XTE for ((a) and (b)) $AB_{l,200}$, ((c) and (d)) $AB_{l,500}$, and ((e) and (f)) $ABp_{,500}$, respectively.

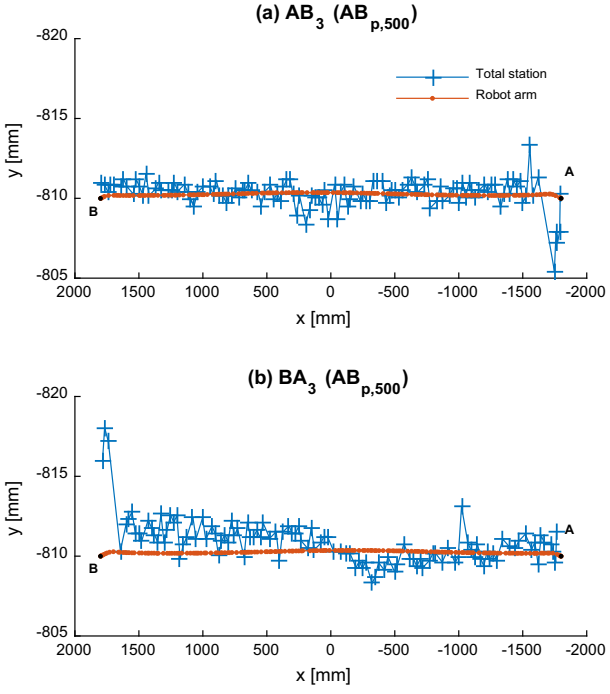

Fig. 9. TS and robotic arm position data in the *xy*-plane for (a) AB_3 and (b) BA_3 of the $AB_{p,500}$ experiment. Points A and B are also indicated (·).

2004; Easterly et al., 2010) and takes into consideration the measured points of the assessing device. The geometrical representation of the relative XTE is presented in Fig. 4. The XTE is the horizontal distance d between any measured position of the prism $p_j^t = (x_j^t, y_j^t)$ $(j = 1, \ldots, k)$ and the specific path of the recorded robotic arm end effector $p_i^r = (x_i^r, y_i^r)$ $(i = 1, \ldots, \xi)$, where k and ξ is the total number of measured points for the prism and the robotic arm, respectively.

In order to find the relative XTE for all measured data, a heuristic algorithm was developed, which for each measured prism point p_j^t was calculating the distance to all points of the robotic arm that belonged to the same path. Subsequently, the two robotic arm points with the smallest distance to p_j^t were chosen as p_{i-1}^r and p_i^r, to find the relative XTE. In order to find the horizontal relative XTE in the *xy*-plane, the procedure was as described above but for the vertical relative XTE in the *xz*-plane, all values of the *y*-axis were replaced with the corresponding values of the *z*-axis.

The computer that was used to execute the heuristic algorithm was a Lenovo T450s laptop with a 64-bit Windows 8.1 Enterprise operating system, equipped with an Intel® Core™ i5-5300U at 2.3 GHz processor, and 12 GB working RAM. The algorithm was developed in MATLAB® R2015b and required 5.6 s to find the vertical and horizontal relative XTE for all performed experiments.

The vector $\mathbf{r}$ that is perpendicular to the line connecting the two reference points p_{i-1}^r and p_i^r is calculated by

$$\mathbf{r} = \begin{bmatrix} y_i^r - y_{i-1}^r \\ -(x_i^r - x_{i-1}^r) \end{bmatrix}.$$

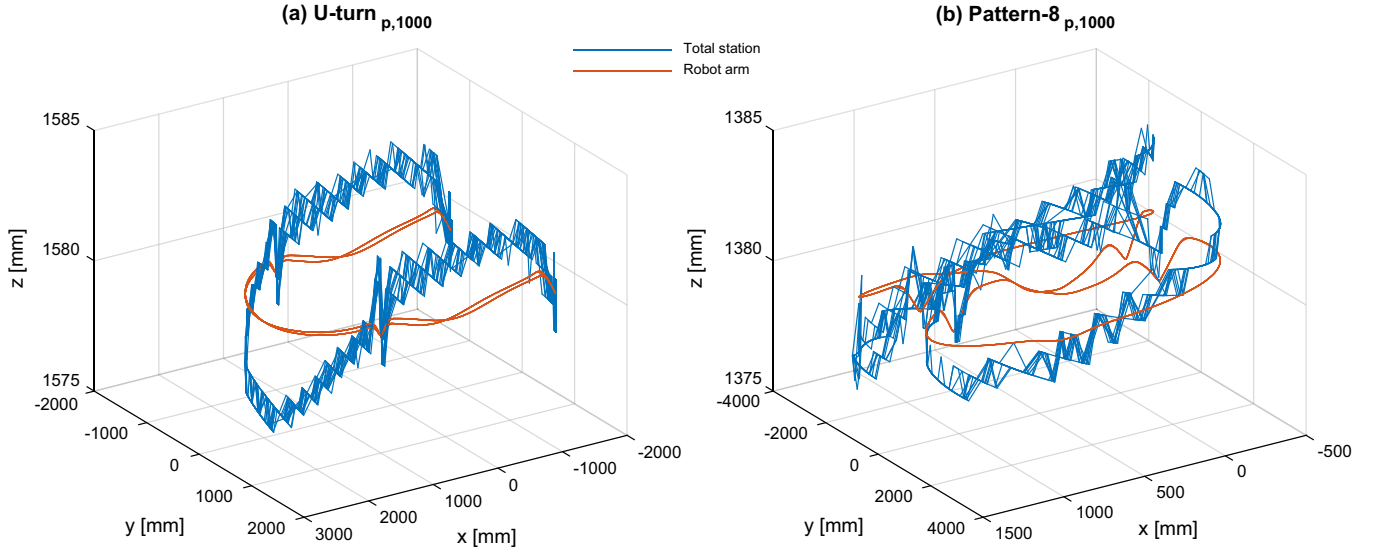

Fig. 10. (a) U-turn and (b) Pattern-8 position data from the TS (blue) and the robotic arm (red). (For interpretation of the references to colour in this figure legend, the reader is referred to the web version of this article.)

Consider $\mathbf{q}$ a vector from the prism position p_j^t to the first robotic arm point p_{i-1}^r defined by

$$\mathbf{q} = \begin{bmatrix} x_{i-1}^r - x_j^t \\ y_{i-1}^r - y_j^t \end{bmatrix},$$

then the relative XTE is equal to the distance d, which is given by projecting $\mathbf{q}$ onto $\mathbf{r}$ provided by

$$d = |\text{proj}_{\mathbf{r}}\mathbf{q}| = |\hat{\mathbf{r}} \cdot \mathbf{q}| = \frac{|\mathbf{r} \cdot \mathbf{q}|}{|\mathbf{r}|} = \frac{|(x_{i-1}^r - x_j^t)(y_i^r - y_{i-1}^r) - (x_i^r - x_{i-1}^r)(y_{i-1}^r - y_j^t)|}{\sqrt{(x_i^r - x_{i-1}^r)^2 + (y_i^r - y_{i-1}^r)^2}} \quad (1)$$

where $\hat{\mathbf{r}}$ is the unit vector in the direction of $\mathbf{r}$.

3. Results and discussion

3.1. Robotic arm performance

The position of the robotic arm end effector in the *xy*-plane for all AB line measurements is presented in Fig. 5, while the mean, standard deviation, and 95th percentile of the absolute error can be seen in Table 3. Due to the lower speed close to points A and B (while accelerating from and decelerating to zero speed), there was a big number of measurements at the beginning and at the end of each path with a small error. This explains the low values for the mean and the standard deviation compared to the corresponding paths that are presented in Fig. 5. The experiment with the lowest speed (i.e. $AB_{l,50}$) had the smallest error. In fact, the deviation for this experiment was lower than the position data resolution and this is why a straight line can be seen in Fig. 5. When the speed was increased (from 50 mm s^{-1} to 200 mm s^{-1} and then to 500 mm s^{-1}), the efficiency of the control algorithm was slightly decreased resulting in a higher absolute deviation, reaching to a value for the 95th percentile of 0.06 mm and 0.32 mm for $AB_{l,200}$ and $AB_{i,500}$ (i = l,p), respectively.

The followed paths of the robotic arm end effector in the *xz*-plane for AB lines, U-turn, and Pattern-8 can be seen in Fig. 6a–c, respectively. The mean, standard deviation, and 95th percentile of the absolute error are presented in Table 4. In Fig. 6a it can be seen that regarding the AB lines, the results were similar to the *xy*-plane: as the speed increased so did the error. The U-turn and the Pattern-8 resulted in a 95th percentile for the absolute error up to 0.65 mm and 1.30 mm, respectively.

3.2. Relative XTE of TS position data

3.2.1. AB line paths

The box plots for horizontal and vertical relative XTE for $AB_{l,50}$ were produced using MATLAB's function *boxplot*, and are presented in Fig. 7a and b, respectively. On each box, the central red[1] line mark is the median, and the edges of the box are the 25th and 75th percentiles. The whiskers extend to the most extreme data value that is not an outlier (approximately $\pm 2.7\sigma$ when data follow a Gaussian distribution), while the outliers are illustrated with a red cross. The same function was used for all described experiments.

For both horizontal and relative XTE, a systematic error was detected when the direction of travel was changed. This was the result of the 180-degree rotation around the z-axis as illustrated in Fig. 3, due to imperfect calibration. The horizontal and vertical relative XTE after the systematic error was removed are presented in Fig. 7c and d, respectively. From Fig. 7c and d can be seen that for $AB_{l,50}$ the whiskers of the horizontal XTE did not exceed 2 mm, while the whiskers of the vertical XTE were higher up to 3 mm with AB_1 path presenting an outlier slightly above 4 mm. The results for the horizontal and vertical relative XTE after the implementation of the Butterworth low-pass filter for noise removal, are presented in Fig. 7e and f, respectively. In this case, and including the outliers, the horizontal relative XTE remained below 2 mm, while the vertical relative XTE did not exceed 3 mm. The same procedure for the systematic error and noise removal was followed for all performed experiment and the final results are presented in the following sections. The only exception was the pattern-8 experiment where no systematic error was detected since a change in direction was not taking place.

The boxplots for $AB_{l,200}$, $AB_{l,500}$, and $AB_{p,500}$ relative XTE are presented in Fig. 8. Again for the $AB_{l,200}$ experiment as the for the $AB_{l,50}$, the whiskers of the horizontal (Fig. 8a) and vertical relative (Fig. 8b) XTE did not exceed 2 mm, and 3 mm, respectively, except for some outliers that can be seen in the vertical XTE. It is evident

[1] For interpretation of color in Fig. 7, the reader is referred to the web version of this article.

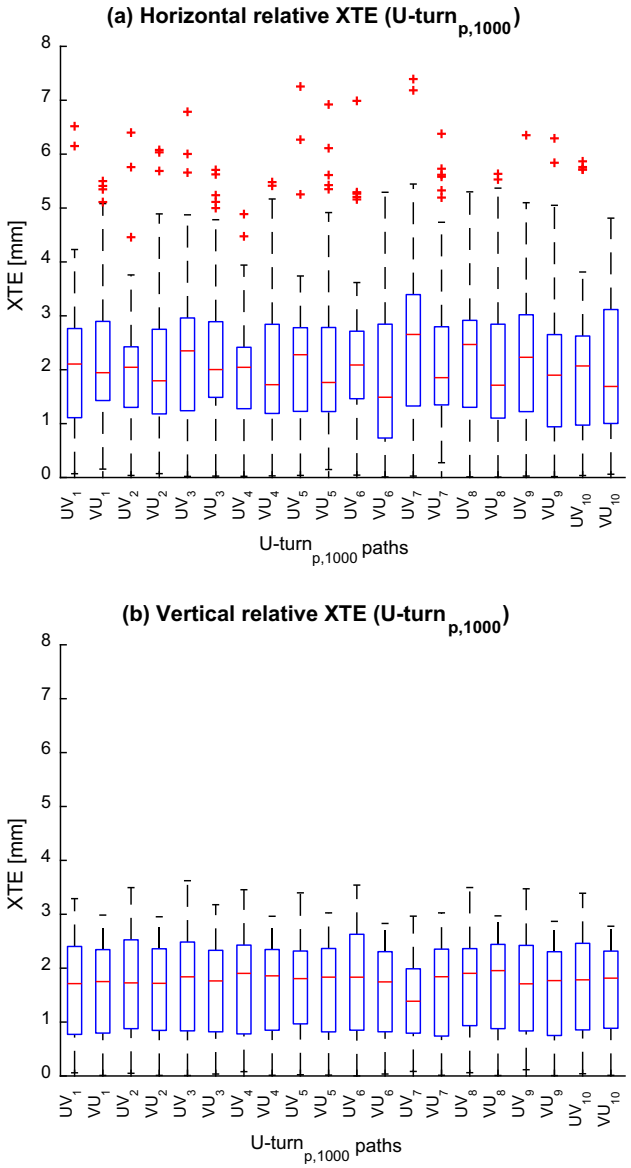

Fig. 11. U-turn$_{p,1000}$ boxplots for (a) horizontal and (b) vertical relative XTE, respectively.

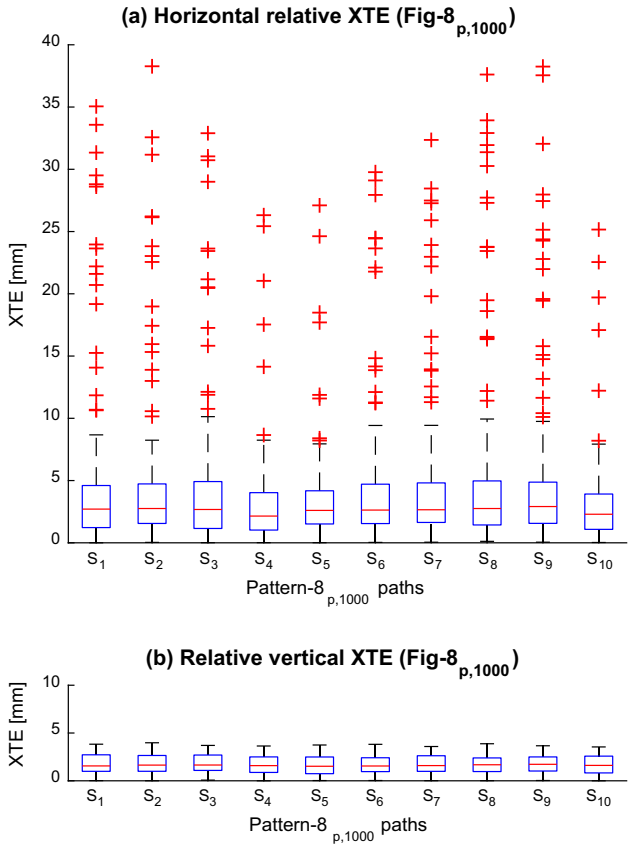

Fig. 12. Pattern-8$_{p,1000}$ boxplots for (a) horizontal and (b) vertical relative XTE, respectively.

that the speed increase from 50 mm s^{-1} to 200 mm s^{-1} did not significantly affect the accuracy of the TS. The former had a slightly better accuracy compared to the latter. For AB$_{l,500}$ experiments, the whiskers of the horizontal relative RTE had a maximum value of around 3 mm (Fig. 8c) with AB$_{p,500}$ having a slightly better performance. Nevertheless, for the AB$_{p,500}$ a high number of outliers is present, reaching up to 16 mm (not illustrated for better comparison of results). The reason for these high-value outliers can be seen in Fig. 9, where an example of the AB and BA lines is illustrated (AB$_3$ and BA$_3$). At the beginning of each path (point A for Fig. 9a, and point B for Fig. 9b), a number of TS measurements had a high relative XTE.

3.2.2. U-turn and Pattern-8

The acquired data from the TS and the robotic arm from the U-turn$_{p,1000}$ and Pattern-8$_{p,1000}$ experiment are illustrated in Fig. 10a and b, respectively. Even from these illustrations, it is obvious that the vertical absolute deviation of the TS from the end effector did not exceed one centimetre since the entire length of the z-axes of Fig. 10a and b is 10 mm. Nevertheless, a difference of the TS data compared to the robotic arm data is easily noticeable and specifically for the Pattern-8 experiment, where a higher error can be noticed at the turning sections compared to the straight parts. The boxplots of the relative XTE for the U-turn$_{p,1000}$ are presented in Fig. 11. From the horizontal relative XTE (Fig. 11a) it is resulted that the error was lower than 10 mm for all paths (including the outliers). The vertical relative XTE for all 20 paths did not exceed 4 mm (Fig. 11b).

The boxplots of the horizontal and vertical XTE for all 10 paths of the Pattern-8 experiment are presented in Fig. 12a and b, respectively. The whiskers of the horizontal relative XTE boxplots reach up to 10 mm but a high number of outliers is detected under all 10 paths. Fig. 12b validates that the vertical relative XTE did not exceed 10 mm for any of the 10 performed paths of Pattern-8, and in fact, it was below 5 mm. In this experiment, no systematic error was detected, as the robotic arm did not change direction during the experiments like the other measurements that had to change from AB to BA (AB-lines) and from UV to VU (U-turn).

3.3. Comparison of all experiments

Using the one-sample Kolmogorov-Smirnov test on each relative XTE dataset, it resulted that none of them followed a normal distribution as for all datasets the null hypothesis was rejected. Consequently, in order to compare the results of the different experiments, the Kruskal-Wallis non-parametric method was utilised, to test whether the datasets originated from the same population. The choice of this method was further supported by the fact that the number of samples for each experiment was different as indicated in Table 5. Furthermore, the Dunn-Šidák post hoc

Table 5
Summary statistics for all performed experiments.

Experiment	Nr. of samples	Horizontal relative XTE [mm]				Vertical relative XTE [mm]			
		Group	Mean	Standard deviation	95th percentile	Group	Mean	Standard deviation	95th percentile
$AB_{l,50}$	6467	A	0.67	0.31	1.16	D	0.92	0.57	1.99
$AB_{l,200}$	5498	A	0.69	0.37	1.24	D	0.89	0.51	1.72
$AB_{l,500}$	2333	B	1.70	0.65	2.53	E	1.51	0.89	2.99
$AB_{p,500}$	2289	A	0.86	1.21	2.06	E	1.46	0.74	2.54
U-$turn_{p,1000}$	2784	B	2.09	1.24	4.30	F	1.65	0.90	3.00
Pattern-$8_{p,1000}$	2156	C	4.01	5.12	12.86	F	1.73	0.99	3.35

approach was used for multiple comparison purposes. The results of this comparison for both horizontal and vertical relative XTE are indicated in the Group column of Table 5. In Table 5, the mean value, the standard deviation, and the 95th percentile of the horizontal and vertical relative XTE for all performed experiments are also presented. As it can be seen, the horizontal relative XTE of the experiments $AB_{l,50}$, $AB_{l,200}$, and $AB_{p,500}$ proved not to be significantly different (group A). Although the $AB_{l,500}$ was performed with the TS at the same position as the $AB_{l,50}$ and $AB_{l,200}$, it was proved that it did not belong to the same group, and not to be significantly different compared to the U-$turn_{p,1000}$ (both belonging to group B). This is reasonable when checking the mean values of these two experiments. For the vertical relative XTE, the multiple comparison showed for the first two experiments not to be significantly different (group D). The rest four experiment were grouped according to their speed: Group E for $AB_{l,500}$ and $AB_{p,500}$, and Group F for U-$turn_{p,1000}$ and Pattern-$8_{p,1000}$.

From Table 5 it is evident that when the speed was increased, the same happened with the horizontal and vertical relative XTE. A big difference can be seen between the U-turn and Pattern-8 experiments. Even though these two experiments were performed with the same speed, and without moving the TS, the latter had a larger mean horizontal relative XTE by 92%, while the standard deviation and the 95th percentile were larger by 313% and 199%, respectively. This was because the Pattern-8 experiment had a bigger part of the route with turning sections than the U-turn experiment, resulting in a higher error. Regarding the vertical relative XTE, the increase in mean, standard deviation, and 95th percentile for these two experiments was smaller, up to 5%, 10%, and 12%, respectively. The reason is that the desired position of the robotic arm on the z-axis was configured to be constant and the motion of the prism that was tracked by the TS did not have turning sections in the xz-plane.

4. Conclusions

From the performed experiments, the resulted accuracy of the TS is very promising in replacing the RTK-GNSS in many applications where a sub-centimetre accuracy of the 3D dynamic position is required. As it was depicted, any systematic error but also measurement noise should be detected and removed from the position data analysis. The mean value of the relative XTE for all experiments had a maximum value of 4.01 mm. The only experiment where the relative XTE exceeded the sub-centimetre level was for Pattern-8 with a value of 12.86 mm for the 95th percentile of the measurements. Of course, this is an extreme case of in-field movement compared to most of the normal agricultural tasks. The vertical relative XTE for all experiments did not exceed 10 mm including the outliers.

Changing the position of the total station, from in-line to perpendicular to the direction of the prism movement, improved the horizontal accuracy of the provided information. It was proved that a number of errors occur when the motion of the prism begins, thus, regarding agricultural applications, it is recommended to start moving and detecting the prism position earlier than the area of interest, i.e. outside plant rows and not directly at the beginning of the rows.

Acknowledgement

The authors are grateful to Dennis Dispot for his support with the robotic arm. Furthermore, they would like to thank the anonymous reviewers for their valuable comments and suggestions to improve the quality of the paper.

References

ANSI/NCSL, 2006. ANSI/NCSL Z540.3-2006 Requirements for the Calibration of Measuring and Test Equipment.

Easterly, D.R., Adamchuk, V.I., Kocher, M.F., Hoy, R.M., 2010. Using a vision sensor system for performance testing of satellite-based tractor auto-guidance. Comput. Electron. Agric. 72, 107–118. http://dx.doi.org/10.1016/j.compag.2010.03.004.

Garrido, M., Paraforos, D., Reiser, D., Vázquez Arellano, M., Griepentrog, H., Valero, C., 2015. 3D maize plant reconstruction based on georeferenced overlapping LiDAR point clouds. Remote Sens. 7, 17077–17096. http://dx.doi.org/10.3390/rs71215870.

Gavric, M., Martinov, M., Bojic, S., Djatkov, D., Pavlovic, M., 2011. Short- and long-term dynamic accuracies determination of satellite-based positioning devices using a specially designed testing facility. Comput. Electron. Agric. 76, 297–305. http://dx.doi.org/10.1016/j.compag.2011.02.008.

Griepentrog, H.W., Nørremark, M., Nielsen, H., Blackmore, B.S., 2005. Seed mapping of sugar beet. Precis. Agric. 6, 157–165. http://dx.doi.org/10.1007/s11119-005-1032-5.

Groth, S., Goldmann, J., Griepentrog, H.W., 2013. Development of a sensing system to assess automatic steering systems. VDI Berichte Nr. 2193, 419–425.

Han, S., Zhang, Q., Noh, H., Shin, B., 2004. A dynamic performance evaluation method for DGPS receivers under linear parallel-tracking applications. Trans. ASAE 47, 321–329.

ISO, 2012. ISO 12188-2:2012 – Tractors and Machinery for Agriculture and Forestry – Test Procedures for Positioning and Guidance Systems in Agriculture – Part 2: Testing of Satellite-based Auto-Guidance Systems During Straight and Level Travel.

ISO, 1998. ISO 9283:1998 - Manipulating Industrial Robots – Performance Criteria and Related Test Methods.

Kirschner, H., Stempfhuber, W., 2008. The kinematic potential of modern tracking total stations - a state of the art report on the leica TPS1200+. In: 1st International Conference on Machine Control & Guidance, pp. 51–60.

Liu, Y., Noguchi, N., 2016. Development of an unmanned surface vehicle for autonomous navigation in a paddy field. Eng. Agric. Environ. Food 9, 21–26. http://dx.doi.org/10.1016/j.eaef.2015.09.003.

Nørremark, M., Griepentrog, H.W., Nielsen, J., Søgaard, H.T., 2008. The development and assessment of the accuracy of an autonomous GPS-based system for intra-row mechanical weed control in row crops. Biosyst. Eng. 101, 396–410. http://dx.doi.org/10.1016/j.biosystemseng.2008.09.007.

Paraforos, D.S., Griepentrog, H.W., Geipel, J., Stehle, T., 2015. Fused inertial measurement unit and real time kinematic-global navigation satellite system data assessment based on robotic total station information for in-field dynamic positioning. In: Stafford, J.V (Ed.), Precision Agriculture '15. Wageningen Academic Publishers, Wageningen, The Netherlands, pp. 275–282. http://dx.doi.org/10.3920/978-90-8686-814-8_33.

Paraforos, D.S., Griepentrog, H.W., Vougioukas, S.G., Kortenbruck, D., 2014. Fatigue life assessment of a four-rotor swather based on rainflow cycle counting. Biosyst. Eng. 127, 1–10. http://dx.doi.org/10.1016/j.biosystemseng.2014.08.006.

Parent, A.C., Bélanger, M.C., Parent, L.E., Santerre, R., Viau, A.A., Anctil, F., Bolinder, M.A., Tremblay, C., 2008. Soil properties and landscape factors affecting maize yield under wet spring conditions in eastern Canada. Biosyst. Eng. 99, 134–144. http://dx.doi.org/10.1016/j.biosystemseng.2007.10.006.

Rose, J., Kicherer, A., Wieland, M., Klingbeil, L., Töpfer, R., Kuhlmann, H., 2016. Towards automated large-scale 3D phenotyping of vineyards under field conditions. Sensors 16, 2136. http://dx.doi.org/10.3390/s16122136.

Ruckelshausen, A., Biber, P., Dorna, M., Gremmes, H., Klose, R., Linz, A., Rahe, R., Resch, R., Thiel, M., Trautz, D., Weiss, U., 2009. BoniRob: an autonomous field robot platform for individual plant phenotyping. In: Precision Agriculture 2009 - Papers Presented at the 7th European Conference on Precision Agriculture, ECPA 2009.

Sama, M.P., Stombaugh, T.S., Lumpp, J.E., 2013. A hardware method for time-stamping asynchronous serial data streams relative to GNSS time. Comput. Electron. Agric. 97, 56–60. http://dx.doi.org/10.1016/j.compag.2013.07.003.

Vougioukas, S.G., He, L., Arikapudi, R., 2016. Orchard worker localisation relative to a vehicle using radio ranging and trilateration. Biosyst. Eng. 147, 1–16. http://dx.doi.org/10.1016/j.biosystemseng.2016.03.006.

Vroegindeweij, B.A., IJsselmuiden, J., van Henten, E.J., 2016. Probabilistic localisation in repetitive environments: estimating a robot's position in an aviary poultry house. Comput. Electron. Agric. 124, 303–317. http://dx.doi.org/10.1016/j.compag.2016.04.019.

Xu, W., Su, Z., Feng, Z., Xu, H., Jiao, Y., Yan, F., 2013. Comparison of conventional measurement and LiDAR-based measurement for crown structures. Comput. Electron. Agric. 98, 242–251. http://dx.doi.org/10.1016/j.compag.2013.08.015.

Yan, F., Ullah, M.R., Gong, Y., Feng, Z., Chowdury, Y., Wu, L., 2012. Use of a no prism total station for field measurements in *Pinus tabulaeformis* Carr. stands in China. Biosyst. Eng. 113, 259–265. http://dx.doi.org/10.1016/j.biosystemseng.2012.08.007.